instruments

MDPI

Article

Output Power Limit in Energy Harvesting Systems Based on Magnetic Induction Incorporating High-Frequency Effects

Yahav Morag * and Yoash Levron

Electrical Engineering Department, Technion - Israel Institute of Technology, Haifa 3200003, Israel; yoashl@ee.technion.ac.il

* Correspondence: yahavm@campus.technion.ac.il

Received: 23 February 2019; Accepted: 17 April 2019; Published: 22 April 2019

Abstract: Wireless power transfer systems based on magnetic induction are usually modeled using the magneto-quasi-static approximation, and by neglecting skin effects and radiation losses. These assumptions imply that the extracted power can grow unlimitedly by increasing frequency or coil size. To bridge this gap, this work proposes general expression for the actual received power of magnetic induction-based energy harvesting transducer, extracting power from a given ambient magnetic field, while accounting for the high-frequency effects. A primary result is that the receiver's output power is inherently limited by radiation losses at high frequencies and impaired by skin and proximity effects at medium frequencies. The approach provides a design tool for estimating the maximal power that can be delivered through a given transducer, and the optimal operating frequency.

Keywords: energy harvesting; magnetic induction; proximity effects; radiation resistance; skin effect

1. Introduction

Energy harvesting has gained much interest in recent years, as a mean to exploit existing ambient energy. Among the various methods developed and available [1,2], magnetic-induction-based energy harvesting (MIEH) takes a significant portion. The operation principle is based on Faraday's law of induction where a voltage is induced in a coil by a time-changing magnetic flux. The source of the magnetic flux can be power lines [3–10], oscillating or vibrating permanent magnets [11–24], variable reluctance [25] or a nearby transmitter coil. Typical applications are condition monitoring sensors powered by power lines [3–7,9,26–28], and powering of biomedical implants [2,14,17,29–32]. In general, the goal is to maximize the output power for a given ambient oscillating magnetic field, i.e., maximize P_{out}/B^2, whereas the particular design challenges vary according to the system constraints [12,26,32–34]. Reference [32] is a book dedicated entirely to wireless power transfer for medical microsystems, which describes with great details the various aspects of the design, including the antenna and the power electronics. In [33], analytical expressions are developed to find the frequencies of maximum transferred power in tightly coupled wireless power transfer systems; however, high-frequency effects are not discussed. Reference [34] describes the realization of a soft flexible coil based on liquid metal alloy for biomedical implantable devices intended for 4 MHz. Reference [35] addresses the system-level design of various micro-scale energy harvesting devices, emphasizes the importance of impedance matching circuit in radio-frequency (RF) energy receiver. In the family MIEH for power lines, reference [4] presents a flexible inductive coil tag for sensing the electric current in the two-wire power cords of household goods for power monitoring. Also for domestic use, [9] describes a MIEH-based power sensor for electrical appliances. Similarly, [5,7] concern energy harvesting from overhead power lines: References [3,5] describes a free-standing inductive harvester to be used in the vicinity of electrical

transmission and distribution equipment, showing that the power density is proportional to the coil diameter and number of turns, and to the frequency squared. In [6,8] different core materials are examined, while in [7], a novel bow-tie-shaped coil is proposed, which is placed under overhead power lines instead of directly on them as in the conventional methods [5,6].

Extracting energy from vibrations of permanent magnets is discussed in [1,11], which analyze and review the use of induction-based transducers both in micro-scale (frequencies up to tens of kHz) and macro scales (frequencies up to hundreds of kHz). Reference [36] provides a novel optimization approach maximizing the output power of such harvesters. Similarly, [17] describes low-frequency (hundreds of Hz) wireless power transfer system for biomedical implants based on rotating permanent magnets. The strong field created by the magnets compensates allows the use of low frequency, which in turns improves the penetration depth, simplifies the impedance matching, and enable the use of high-permeability cores to further enhance the coupling. Reference [2] reviews a variety of techniques to harvest energy for implantable biosensors, with a focus on the inductive link. It shows that this method is advantageous for powering implanted devices in terms of achievable power levels per size, the absence of moving parts, and the possibility for bidirectional data communication. Reference [29] describes a wireless power transfer system integrated for colon inspection at a frequency of 216 kHz. Reference [37] presents a closed-loop inductive powering link for wireless cortical implants. The operating frequency was chosen as 8 MHz, as a compromise between high power transfer efficiency, the low absorption at the tissues, and the gate losses at the power amplifier. Reference [38] describes the design and optimization of four-coil wireless power delivery systems for biomedical implants, operating at 700 kHz. It was shown to provide higher performance in terms of power efficiency and working distance, compared to the conventional two-coil system.

MIEH systems are usually modeled using the magneto-quasi-static approximation. Under this assumption, high-frequency (HF) effects associated with far-field radiation are not explicitly incorporated. Additionally, skin and proximity effects in coil conductors are usually ignored when evaluating maximal receiver output power. Under these approximations, the received power can grow unlimitedly by increasing coil size (cross-section and number of turns) or operating frequency. However, as shown in this work, such a conclusion may be misleading and often results in a non-optimal choice of operational frequency or coil structural parameters. Having said that, the vast majority of the existing literature concerns relatively low frequencies, i.e., in the order of a few megahertz or lower [2]. Moreover, in many cases, the quasistatic approach is very reasonable, e.g., when extracting energy from power lines (50–60 Hz), or in rotating permanent magnets. Nevertheless, it may be of interest to examine the limit of extracted power limit from a theoretical point of view, hence, a wider frequency band is considered, in which that assumption may no longer hold. Among the existing literature, references [2,30,31] did address HF aspects of induction power transfer. Reference [2] confirmed that the optimum frequency for wireless power transmission for implantable devices is in the gigahertz range, as originally described by [30,31], significantly higher than the common frequencies used for wireless power transfer [2]. Although [30,31] performs full-wave analysis, skin and proximity effects within the coil itself were not discussed. These HF aspects were partly addressed by the authors in the context of magnetic sensors [39] and induction power transfer systems [40].

The objective of this study is, therefore, to extend previous works [31,39,40], and develop a strict limit for the extracted power in MIEH systems while accounting for the HF effects. Maximal available output power is mapped as a function of frequency, and the optimal operating frequency is then derived. One main result is that the potentially extracted power in MIEH systems cannot grow unlimitedly by either enlarging the coil's structural parameters or by increasing the frequency. It is shown that the monotonic rise of extracted power with frequency eventually reaches a maximum point, in which radiation loss becomes dominant. Beyond this peak frequency, power descends regardless of coil parameters. A large coil may extract more power than a small coil. However, it will reach its power maximum at a lower frequency so that small coils may have an advantage at higher frequencies.

2. Maximal Received Power in Receiver Coil Subjected to a Given Ambient Magnetic Field

In this section, expressions for received power in the MIEH system, comprised of a receiver coil maintained in a given ambient magnetic field, are derived. Figure 1a displays a coil of N turns with a wire diameter d_w, winded at a r_{av} average radius around a high-permeability, low-conductivity core. The coil is connected to a load impedance, marked z_l. The core has apparent (also termed as equivalent, or effective) permeability μ_{app}, representing the amount of flux concentrated into the core. μ_{app} is a function of the material permeability, μ_{rc}, the core geometry and aspect ratio [41–43]. The MIEH receiver is subjected to a time-harmonic magnetic field H, assumed to be directed along the coil axis.

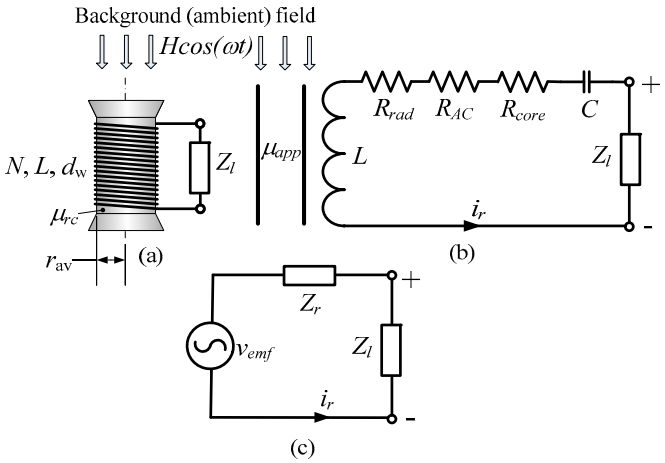

Figure 1. Basic MIEH transducer. (**a**) General view. (**b**) Circuit representation. (**c**) The actual equivalent circuit.

Figure 1b,c show the equivalent circuit. This circuit is excited by the induced voltage v_{emf}. The passive elements are the coil self-inductance L, the wire inductance L_{w}, the AC loss (Ohmic) resistance R_{AC}, and the self-capacitance C. The core losses (due to eddy currents and hysteresis), as well as the coil radiation resistance, are represented by the equivalent resistors R_{core} and R_{rad}, respectively.

The induced voltage in the coil v_{emf} is proportional to the rate of change of the magnetic flux ϕ, and the number of turns N:

$$v_{emf} = -N\frac{\partial \phi}{\partial t} \tag{1}$$

where:

$$\frac{\partial \phi}{\partial t} = \frac{\partial}{\partial t}\left(\vec{B}\cdot\vec{A}\right) = \mu_0\mu_{app}A\frac{\partial H}{\partial t} \tag{2}$$

Since $A = \pi {r_{av}}^2$, then the peak induced voltage is:

$$v_{emf} = 2\pi^2 N r_{av}^2 f \mu_0 \mu_{app} H \tag{3}$$

Hence, v_{emf} is proportional to $N{\cdot}{r_{\text{av}}}^2$. The relation between the ambient field H and the ambient magnetic flux density B is given by:

$$B = \mu_0 H \tag{4}$$

A permeable core will attract and confine the surrounding flux lines inside it, so the magnetic flux density sensed by coil B_{in} will be amplified by μ_{app}. Hence:

$$B_{in} = \mu_{app} B \tag{5}$$

The peak induced voltage (3) can now be written as a function of ambient field B, such as:

$$v_{emf} = 2\pi^2 N r_{av}^2 f \mu_{app} B \tag{6}$$

Designating the input impedance of the receiver as z_r:

$$z_r \equiv R_{AC} + R_{rad} + R_{core} + \frac{1-\omega^2 LC}{j\omega C} \tag{7}$$

The voltage equation is:

$$v_{emf} - (z_r + z_l) i_r = 0 \tag{8}$$

The receiver should be tuned to resonate at the ambient field frequency to minimize impedance and maximize power transfer. This means that $LC = 1/\omega_0^2$, so the coil reactances cancel each other:

$$z_r \equiv R_{AC} + R_{rad} + R_{core} \tag{9}$$

Additionally, load impedance should equal the complex conjugate of the receiver's input impedance, such as,

$$z_l = z_r^* \tag{10}$$

yielding:

$$v_{emf} - 2(R_{AC} + R_{rad} + R_{core}) \cdot i_r = 0 \tag{11}$$

Using (3) and (8), the time-average normalized output power (dissipated at the load power) is finally obtained:

$$\frac{P_{out}}{B^2} = \frac{1}{2}\frac{i_r^2 z_l}{B^2} = \frac{1}{2} \cdot \frac{\pi^4 N^2 r_{av}^4 \mu_{app}^2 f_0^2}{(R_{AC} + R_{rad} + R_{core})} \left[\frac{\mathrm{W}}{\mathrm{T}^2}\right] \tag{12}$$

where i_r is the peak current, B is the peak ambient field and $f_0 = \omega_0/2\pi$ is the resonance frequency. It is easy to see that the assumption of DC resistance ($\propto N \cdot r_{av}$), with no radiation and core losses, yields a received power that is proportional to $f^2 \cdot N \cdot r_{av}^3$. Apparently, the power can be increased at will, either by enlarging coil radius, adding more turns, or increasing frequency. However, as the next sections will show, this is not the case, since the radiation term sets an upper limit on this power.

3. Resistance Terms of the Equivalent Circuit

Explicit expressions for the resistance terms of the circuit (i.e., R_{AC}, R_{rad}, and R_{core}) are each described in detail in [39]. The coil Ohmic resistance increases drastically with frequency, due to skin and proximity effects. The coil DC resistance is approximated as [39]:

$$R_{DC} \approx \frac{8 N r_{av}}{\sigma d_w^2} \tag{13}$$

where d_w is the wire diameter. The overall coil resistance, accounting for skin effect is derived in [39], based on [44]:

$$R_{AC_{skin}} \approx \frac{\pi \mu_0 \mu_r N r_{av}}{[r_0/\delta + e^{-r_0/\delta} - 1]} f \tag{14}$$

where r_0 is the wire radius ($r_0 = d_w/2$) and δ is the skin depth, given by $\delta = 1/\sqrt{(\pi \mu_0 \mu_r \sigma f)}$. Here, σ and μ_{r} are the specific conductivity and permeability of the wire material, respectively. At low relative frequencies ($\delta \gg r_0$), $R_{\mathrm{AC}} = R_{\mathrm{DC}}$, while in high relative frequencies ($\delta \ll r_0$), R_{AC} reduces to $(r_0/2\delta)R_{\mathrm{DC}}$.

In a multi-turn, multi-layer coil, mutual influence of fields from nearby conductors, known as proximity effect, increases resistance even further. Reference [45] provides a semi-analytical formula for the overall AC/DC resistance ratio of a multi-turn, multi-layer coil. Based on this formula, the overall Ohmic resistance of the coil is [39]:

$$R_{AC} = R_{AC_{skin}} + \left[\frac{1}{4}\left(\frac{kb}{D}m\right)^2 \left(\frac{d_w}{c_{gap}}\right)^2 G\right] R_{DC} \tag{15}$$

In (15), G is the proximity effect factor, given by a look-up table [45] according to r_0 and δ. D and b are the coil's outer diameter and length, respectively. The coefficient k is found graphically [45] according to the ratios D/b and t/D, where t is the coil's radial thickness [45]. The number of winding radial layers is designated by m, and c_{gap} is the spacing between the centers of adjacent turns in the same layer (Figure 2 [39]).

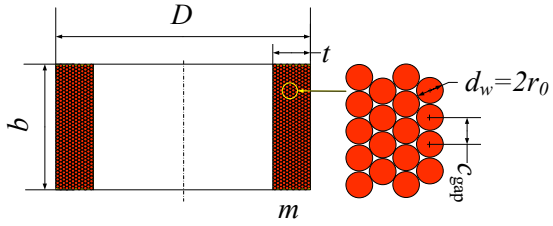

Figure 2. Geometric parameters used in (15) [39].

Reference [39] facilitates the incorporation of the proximity effect into analytical power expressions, by formulating G as a function of r_0/δ, using the look-up table given in [45] for two non-dimensional frequency zones:

$$\begin{cases} G_{LF} \approx 0.05\left(\frac{r_0}{\delta}\right)^2 & r_0/\delta \le 1 \\ G_{HF} \approx 0.25\left(\frac{r_0}{\delta}\right) - 0.2 & r_0/\delta > 1 \end{cases} \tag{16}$$

Resistance amplification due to the proximity effect is expressed by the *proximity effect factor* k_{prox} [39]:

$$k_{prox} = \frac{R_{AC}}{R_{AC_{skin}}} = 1 + \frac{1}{4}\left(\frac{kb}{D}m\right)^2\left(\frac{d_w}{c_{gap}}\right)^2 G\frac{R_{DC}}{R_{AC_{skin}}} \tag{17}$$

The maximal value of k_{prox} per a given coil is given by [39]:

$$k_{prox_{\max}} \approx 1 + \frac{1}{8}\left(\frac{kb}{D}m\right)^2\left(\frac{d_w}{c_{gap}}\right)^2 \tag{18}$$

The radiation resistance R_{rad} expresses the radiated power to the surrounding space. Based on [46] and [47], the free-space radiation resistance of induction coil, winded on a permeable core is [39]:

$$R_{rad} = \left(\frac{8\mu_0\pi^5}{3c^3}\right)\mu_{app}^2 r_{av}^4 N^2 f^4 \tag{19}$$

According to the *Carson Reciprocity theorem*, if the media is linear, passive and isotropic [48], then the transmitting and receiving patterns of an antenna are the same. Also, for matched impedances, the power flow is the same either way, meaning that the radiation resistance of the MIEH coil is according to (19). The radiation resistance term is negligible at low frequency but rises sharply as the frequency increases, due to the fourth power. Additionally, this sharp rise will occur much earlier for large coils (radius, the number of turns) than for small ones.

Like the Ohmic loss within the coil, the high-permeability core material (if used) is an additional source of power dissipation. Principal loss mechanisms are hysteresis and eddy current losses, all rise with frequency. In this work, however, we assume small core losses compared to copper losses (i.e., $R_{\text{core}} \approx 0$). We justify this by assuming a low-intensity field and a core material with a narrow hysteresis loop, high electrical resistance, and thin laminations to reduce both hysteresis and eddy current losses.

4. Explicit Power Expressions

After deriving the explicit expressions for resistance terms R_{AC} and R_{rad}, we substitute them into (12) to get the explicitly normalized load power under resonance condition:

$$\frac{P_{out}}{B^2} = \frac{1}{2} \cdot \frac{\pi^3 N r_{av}^3 \mu_{app}^2 f_0}{\frac{k_{prox}\mu_0\mu_r}{\left[r_0/\delta + e^{-r_0/\delta} - 1\right]} + \left(\frac{8\pi^4}{3c^3}\right)\mu_0 \mu_{app}^2 r_{av}^3 N f_0^3} \tag{20}$$

where $f_0 = 1/2\pi\sqrt{LC}$, and $B = \mu_0 H$ is the surrounding field. At low relative frequencies ($\delta \gg r_0$), $R_{AC} \approx R_{DC} \gg R_{rad}$, thus (20) becomes:

$$\frac{P_{out}}{B^2} \approx \frac{\pi^4 N^2 r_{av}^4 \mu_{app}^2 f_0^2}{2R_{DC}} \tag{21}$$

Hence, the load power at low frequencies becomes:

$$\left.\frac{P_{out}}{B^2}\right|_{\delta \gg r_0} \approx \left(\frac{\pi^4\sigma}{16}\right)\left(d_w^2 N r_{av}^3 \mu_{app}^2\right) \cdot f_0^2 = \left(\frac{\pi^4\sigma}{16}\right)(CF)^4 \cdot f_0^2 \tag{22}$$

where CF is the "*Coil-factor*" [39] and expresses coil size in a concentrated manner:

$$CF \equiv d_w^{0.5} N^{0.25} r_{av}^{0.75} \mu_{app}^{0.5} \tag{23}$$

Equation (22) suggest that load power at low frequencies can grow unlimitedly with the growth of structural parameters (N, r_{av}, d_w, and μ_{app}). This conclusion is, of course, a non-physical one, resulting from the DC approximation neglecting the HF effects.

At the other extreme (i.e., at sufficiently high frequencies in which $\delta \ll r_0$, $R_{rad} \gg R_{AC}$, thus (20) becomes:

$$\left.\frac{P_{out}}{B^2}\right|_{\delta \ll r_0} \approx \left(\frac{3c^3}{16\pi\mu_0}\right) \cdot \frac{1}{f_0^2} \tag{24}$$

At high frequencies, and unlike the low-frequency regime, all coil lines drain together into a single line, independent of coil parameters, which decreases as f_0^{-2}.

The peak frequency, where the power is maximal, is estimated by the intersection point of the two asymptotic lines:

$$f_{peak} \approx \sqrt[4]{\frac{3c^3}{\mu_0\pi^5\sigma}} \cdot \frac{1}{\sqrt[4]{d_w^2 N r_{av}^3 \mu_{app}^2}} = \sqrt[4]{\frac{3c^3}{\mu_0\pi^5\sigma}} \cdot \frac{1}{CF} \tag{25}$$

Moreover, the related supreme power:

$$\left.\frac{P_{out}}{B^2}\right|_{\max} \approx \sqrt{\frac{3\pi^3 c^3 \sigma}{256\mu_0}} \sqrt{d_w^2 N r_{av}^3 \mu_{app}^2} = \sqrt{\frac{3\pi^3 c^3 \sigma}{256\mu_0}} (CF)^2 \tag{26}$$

From (25) and (26), it is observed that large coils are more potent than small ones, yet reach their ultimate power at a lower frequency.

5. Results

A numerical simulation was conducted to examine the above results. Figure 3 shows the time-average output power P_{out}/B^2 for four coils with CF ranging from 10 to 10,000 $\mathrm{mm}^{1.25}$ (here, r_{av} and d_w are given in mm just for convenience; however, in (22)–(26), the units of CF must be consistent with other parameters in the expression). The four colored solid lines represent the power when accounting for skin effect and radiation resistance, but with no proximity effect ($k_{\mathrm{prox}} = 1$). For the

largest value (CF = 10,000 mm$^{1.25}$—blue line), we exhibit the additional two asymptotic lines (22) and (24), representing the low- and high-frequency end cases. For that coil, we also show the power limit with proximity effect included (blue dashed line). This coil is assumed to have the following data: N = 4000 turns, r_{av} = 1000 mm, d_w = 1 mm, and μ_{app} = 50 (all leading to CF = 10,000 mm$^{1.25}$). For the proximity effect, we assumed m = 10 layers, kb/D = 7, and d_w/c_{gap} = 1. Due to the large number of radial layers, the proximity effect causes major power degradation ($k_{\text{prox\_max}}$ ~ 613), as illustrated by the existing gap between the two blue lines.

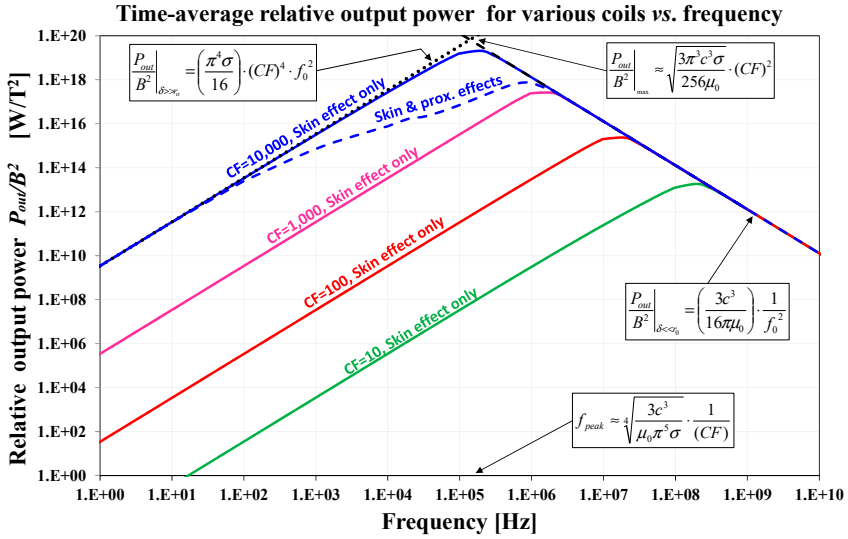

Figure 3. Time-average relative powers for four coils differ in size. For the largest coil (CF = 10,000 mm$^{1.25}$), also shown are the asymptotic lines that characterize the low-frequency and high-frequency behaviors along with the influence of 'with proximity' effect.

6. Discussion

The above analysis demonstrates that each MI receiver, when tuned to operate at resonance and with matched impedance, has an upper bound for its potential extracted power. The frequency dependence can be characterized by three different modes, as seen in Figure 3. In the low-frequency band, power is constrained by the DC resistance. In that zone, received power improves as the coil becomes larger in any of the structural aspects (larger area, more turns, thicker wire, and higher permeability), as expressed by the coil-factor. In this zone, power grows as f_0^2. At a certain point, proximity and skin effects begin to impair received power (blue dashed line). The exact inception point depends on coil-specific winding parameters (15). This behavior continues until peak frequency f_{peak} (26), at which the power reaches its highest value (26). The slightly curved shape of the peak is the result of the skin effect. At the peak point, radiation resistance becomes the dominant resistance term and causes a trend reversal: Power starts decreasing with a constant slope proportional to $1/{f_0}^2$, independent of coil parameters. Hence, all power lines are drained into a single line.

7. Comparison with Existing Literature

Let us compare the obtained results with those described by [31], which addressed HF induction power transfer. It considered a receiving single-turn loop with an area of 4 mm^2. The wire has a trace width of 0.20 mm and trace thickness of 0.04 mm. These values can be translated to d_w = 1.009 mm and r_{av} = 1.128 mm. Since no core is used μ_{app} = 1. Hence, CF is calculated according to (23) as 1.1 mm$^{1.25}$. The resulted peak frequency (25) is 2.98 GHz, compared to about 2.5 GHz in [31]. Although [31] considered the efficiency of a transmitter-receiver system, and this paper considers the receiver alone, the results are in the same order of magnitude, and present a similar behavior, while the difference can be attributed to the conductivity of the tissue.

8. Summary and Conclusions

This paper addressed the power output limits of magnetic MIEH devices, providing a simple expression for the output power as a function of various design parameters and operating frequency. It is shown that relative output power deteriorates due to skin and proximity effects and is fundamentally limited by radiation losses. The power-frequency dependency (Figure 3) is characterized by a triangular shape. At low frequencies, power rises with f_0^2 and depends strongly on the coil parameters, as expressed by the "Coil-factor" (23). For a multi-turn coil, this output power is reduced as a result of skin and proximity effects. Due to the dominance of radiation resistance at high frequencies, the power reaches a maximum point at f_{peak} (25) and then descends in proportion to ${f_0}^{-2}$, independent of coil parameters.

Author Contributions: Y.M. received his Ph.D. degree in 2018 in electrical engineering at the Technion-Israel Institute of Technology, Haifa, Israel. His research was conducted under the supervision of Y.L. and focused on optimization of magnetic sensing, wireless power transfer and magnetic communication systems based on magnetic induction.

Conflicts of Interest: The authors declare no conflict of interest.

References

1. Shashank Priya, E.; Inman, D.J. *Energy Harvesting Technologies*; Springer Science+Business Media: New York, NY, USA, 2009.
2. Olivo, J.; Carrara, S.; de Micheli, G.; de Micheli, G. Energy Harvesting and Remote Powering for Implantable Biosensors. *IEEE Sens. J.* **2011**, *11*, 1573–1586. [CrossRef]
3. Roscoe, N.; Judd, M.D.; Fitch, J. Development of magnetic induction energy harvesting for condition monitoring. In Proceedings of the 44th International Universities Power Engineering Conference (UPEC), Glasgow, UK, 1–4 September 2009; pp. 1–5.
4. Chen, Y.-C.; Yu, S.-C.; Cheng, S.-H.; Cheng, Y.-T. A Flexible Inductive Coil Tag for Household Two-Wire Current Sensing Applications. *IEEE Sens. J.* **2012**, *12*, 2129–2134. [CrossRef]
5. Roscoe, N.M.; Judd, M.D. Harvesting Energy from Magnetic Fields to Power Condition Monitoring Sensors. *IEEE Sens. J.* **2013**, *13*, 2263–2270. [CrossRef]
6. Santos, M.P.D.; Vieira, D.A.; Rodriguez, Y.P.M.; de Souza, C.P.; de Moraes, T.O.; Freire, R.C.S. Energy harvesting using magnetic induction considering different core materials. In Proceedings of the 2014 IEEE International Instrumentation and Measurement Technology Conference (I2MTC), Montevideo, Uruguay, 12–15 May 2014; pp. 942–944.
7. Yuan, S.; Huang, Y.; Zhou, J.; Xu, Q.; Song, C.; Thompson, P. Magnetic Field Energy Harvesting Under Overhead Power Lines. *IEEE Trans. Power Electron.* **2015**, *30*, 6191–6202. [CrossRef]
8. Vieira, D.A.; Santos, M.P.; Costa, A.C.F.M.; Souza, C.P. Ni-Zn Ferrite Core Characterization for Magnetic-based Energy Harvesting Application. *IEEE Lat. Am. Trans.* **2016**, *14*, 4070–4075. [CrossRef]
9. Tsunoda, Y.; Tsuchiya, C.; Segawa, Y.; Sawaya, H.; Hasegawa, M.; Ishigaki, S.; Ishibashi, K. A small-size energy-harvesting electric power sensor for implementing existing electrical Appliances into HEMS. *IEEE Sens. J.* **2016**, *16*, 457–463. [CrossRef]
10. Jiang, W.; Lu, J.; Li, F.; Hashimoto, S.; Lin, Z. A non-intrusive magnetic energy scavanger for renewable power generation state monitoring. In Proceedings of the 2016 IEEE International Conference on Renewable Energy Research and Applications (ICRERA), Birmingham, UK, 20–23 November 2016; Volume 5, pp. 562–566.
11. Arnold, D.P. Review of microscale magnetic power generation. *IEEE Trans. Magn.* **2007**, *43*, 3940–3951. [CrossRef]
12. Priya, S.; Inman, D.J. Electromagnetic energy harvesting. In Proceedings of the International Conference on Robotics and Mechatronics (IcRoM 2018), Tehran, Iran, 23–25 October 2018; pp. 322–325.
13. Mallick, D.; Paul, K.; Roy, S. Design Optimization of Fully Integrated, MEMS Electromagnetic Energy Harvesting Devices using Patterned Micro-magnet Arrays. In Proceedings of the 2018 IEEE 18th International Conference on Nanotechnology (IEEE-NANO), Cork, Ireland, 23–26 July 2018; pp. 1–3.

14. Gulbahar, B. Energy Harvesting and Magneto-Inductive Communications With Molecular Magnets on Vibrating Graphene and Biomedical Applications in the Kilohertz to Terahertz Band. *IEEE Trans. Mol. Biol. Multi-Scale Commun.* **2018**, *3*, 194–206. [CrossRef]
15. Li, C.; Shuai, W.; Luk, P.; Gu, M.; Jiao, Z. Enhanced Bandwidth Nonlinear Resonance Electromagnetic Human Motion Energy Harvester Using Magnetic-Springs and Ferrofluid. *IEEE/ASME Trans. Mechatronics* **2019**, *24*, 710–717. [CrossRef]
16. Roy, S.; Mallick, D.; Paul, K. MEMS-Based Vibrational Energy Harvesting and Conversion Employing Micro-/Nano-Magnetics. *IEEE Trans. Magn.* **2019**, *PP*, 1–15. [CrossRef]
17. Jiang, H.; Zhang, J.; Lan, D.; Chao, K.K.; Liou, S.; Shahnasser, H.; Fechter, R.; Hirose, S.; Harrison, M.; Roy, S. A low-frequency versatile wireless power transfer technology for biomedical implants. *IEEE Trans. Biomed. Circuits Syst.* **2013**, *7*, 526–535. [CrossRef] [PubMed]
18. Zhang, Q.; Kim, E.S. Vibration energy harvesting based on magnet and coil arrays for watt-level handheld power source. *Proc. IEEE* **2014**, *102*, 1747–1761. [CrossRef]
19. Zhang, Q.; Kim, E.S. Micromachined energy-harvester stack with enhanced electromagnetic induction through vertical integration of magnets. *J. Microelectromech. Syst.* **2015**, *24*, 384–394. [CrossRef]
20. Khan, F.U.; Iqbal, M. Electromagnetic-based bridge energy harvester using traffic-induced bridge's vibrations and ambient wind. In Proceedings of the 2016 International Conference on Intelligent Systems Engineering (ICISE), Islamabad, Pakistan, 15–17 January 2016; pp. 380–385.
21. Gatti, R.R.; Howard, I.M.; Lumentut, M.F. Design and simulation of core-ring magnet configurations for maximising energy transduction in linear actuators and micro-energy generators. In Proceedings of the 2016 International Conference on Energy Efficient Technologies for Sustainability (ICEETS), Nagercoil, India, 7–8 April 2016; pp. 796–801.
22. Lee, B.-C.; Chung, G.-S. Design and analysis of a pendulum-based electromagnetic energy harvester using anti-phase motion. *IET Renew. Power Gener.* **2016**, *10*, 1625–1630. [CrossRef]
23. Torres, E.; Ponce, P.; Molina, A. Electromagnetic induction generator toward energy harvesting for dynamic systems. In Proceedings of the 2017 IEEE International Conference on Industrial Technology (ICIT), Toronto, ON, Canada, 22–25 March 2017; pp. 418–422.
24. Buccolini, L.; Conti, M. An Energy Harvester Interface for Self-Powered Wireless Speed Sensor. *IEEE Sens. J.* **2017**, *17*, 1097–1104. [CrossRef]
25. Xu, Y.; Bader, S.; Oelmann, B. A Survey on Variable Reluctance Energy Harvesters in Low-Speed Rotating Applications. *IEEE Sens. J.* **2018**, *18*, 3426–3435. [CrossRef]
26. Silva, M.T.P.; Vasconcelos, F.X.E.V.H. Temperature sensing system with short-range wireless sensor based on inductive coupling. *IEEE Sens. J.* **2011**, *11*, 2469–2478. [CrossRef]
27. Leon-salas, W.D.; Halmen, C. A RFID sensor for corrosion monitoring in concrete. *IEEE Sens. J.* **2016**, *16*, 32–42. [CrossRef]
28. Salas, M.; Focke, O. Wireless power transmission for structural health monitoring of fiber-reinforced-composite materials. *IEEE Sens. J.* **2014**, *14*, 2171–2176. [CrossRef]
29. Chen, W.; Yan, G.; He, S.; Ke, Q.; Wang, Z.; Liu, H. Wireless powered capsule endoscopy for colon diagnosis and treatment. *Physiol. Meas.* **2013**, *34*, 1545–1651. [CrossRef]
30. Poon, A.S.Y.; O'Driscoll, S.; Meng, T.H. Optimal operating frequency in wireless power transmission for implantable devices. In Proceedings of the 2007 29th Annual International Conference of the IEEE Engineering in Medicine and Biology Society, Lyon, France, 22–26 August 2007; pp. 5673–5678.
31. Poon, A.S.Y.; O'driscoll, S.; Meng, T.H. Optimal frequency for wireless power transmission into dispersive tissue. *IEEE Trans. Antennas Propag.* **2010**, *58*, 1739–1750. [CrossRef]
32. Sun, T.; Xie, X.; Wang, Z. *Wireless Power Transfer for Medical Microsystems*, 1st ed.; Springer: New York, NY, USA; Heidelberg, Germany; Dordrecht, The Netherlands; London, UK, 2013.
33. Kong, S.; Kim, M.; Koo, K.; Ahn, S.; Bae, B.; Kim, J. Analytical expressions for maximum transferred power in wireless power transfer systems. In Proceedings of the 2011 IEEE International Symposium on Electromagnetic Compatibility, Long Beach, CA, USA, 14–19 August 2011; pp. 379–383.
34. Qusba, A.; RamRakhyani, A.K.; So, J.-H.; Hayes, G.J.; Dickey, M.D.; Lazzi, G. On the design of microfluidic implant coil for flexible telemetry system. *IEEE Sens. J.* **2014**, *14*, 1074–1080. [CrossRef]
35. Lu, C.; Raghunathan, V.; Roy, K. Efficient design of micro-scale energy harvesting systems. *IEEE J. Emerg. Sel. Top. Circuits Syst.* **2011**, *1*, 254–266. [CrossRef]

36. Cepnik, C.; Wallrabe, U.; Radler, O.; Rosenbaum, S.; Strohla, T. On a novel optimization approach of electromagnetic energy harvesters. In Proceedings of the 2011 Fourth International Conference on Modeling, Simulation and Applied Optimization, Kuala Lumpur, Malaysia, 19–21 April 2011; Volume 1, pp. 1–6.
37. Silay, K.M.; Dehollain, C.; Declercq, M. A closed-loop remote powering link for wireless cortical implants. *IEEE Sens. J.* **2013**, *13*, 3226–3235. [CrossRef]
38. Ramrakhyani, A.K.; Mirabbasi, S.; Chiao, M. Design and optimization of resonance-based efficient wireless power delivery systems for biomedical implants. *IEEE Trans. Biomed. Circuits Syst.* **2011**, *5*, 48–63. [CrossRef]
39. Morag, Y.; Tal, N.; Nazarathy, M.; Levron, Y. Thermodynamic Signal to Noise and Channel Capacity Limits of Magnetic Induction Sensors and Communication Systems. *IEEE Sens. J.* **2016**, *16*, 1575–1585. [CrossRef]
40. Morag, Y.; Tal, N.; Levron, Y. Power Transfer Limits and optimal operation frequency in Induction Power Transfer Systems Incorporating High-frequency effects. In Proceedings of the 2016 International Symposium on Power Electronics, Electrical Drives, Automation and Motion (SPEEDAM), Anacapri, Italy, 22–24 June 2016; pp. 79–84.
41. Śran, H.C.; Fergeau, P. An optimized low-frequency three-axis search coil magnetometer for space research. *Rev. Sci. Instrum.* **2005**, *76*, 1–10.
42. Slawomir, T. Induction coil sensors—A review. *Meas. Sci. Technol.* **2007**, *18*, R31.
43. Coillot, C.; Leroy, P. Induction Magnetometers Principle, Modeling and Ways of Improvement. In *Magnetic Sensors Principles and Applications*; Kuang, K., Ed.; InTechOpen: Rijeka, Croatia, 2012.
44. Lehner, G. Time-dependent problems I (Quasi-stationary approximation). In *Electromagnetic Field Theory for Engineers and Physicists*; Springer: Berlin/Heidelberg, Germany, 2010; pp. 369–404.
45. Terman, F.E. Inductance and mutual inductance. In *Radio Engineer's Handbook*; McGraw-Hill Book Company: New York, NY, USA, 1943; Volume 28, pp. 60–62.
46. Balanis, C.A. Loop antenna. In *Antenna Theory-Analysis and Design*; John Wiley & Sons, Inc.: Hoboken, NJ, USA, 2005; pp. 231–260.
47. Kraus, J.D.; Marhefka, R.J. The loop antenna. In *Antennas for All Applications*, 3rd ed.; McGraw-Hill Book Company: New York, NY, USA, 2002; pp. 217–219.
48. Kraus, J.D.; Marhefka, R.J. Self and mutual impedances. In *Antennas for All Application*; McGraw-Hill Book Company: New York, NY, USA, 2002; pp. 438–440.